*Original Paper*

# Depth Distribution of Photoelectron Yield Calculated by Multiple Scattering Theory

H. Shinotsuka*, H. Arai and T. Fujikawa
*Graduate School of Advanced Integration Science,*
*Chiba University, Yayoi-cho 1-33, Inage, Chiba 263-8522,Japan*
**shino@graduate.chiba-u.jp*

(Received: November 26, 2007; Accepted: December 18, 2007)

The emission depth distribution function (EDDF) $\phi(z)$ in normal photoemission from solids is studied by use of quantum full multiple scattering theory and non-hermitian optical potential $\Sigma$. The present theoretical approach explicitly takes the details of atomic arrangement in solids into account, which is in contrast to the currently used classical approaches applied to jellium models. The latter approach cannot study the interference effects caused by the elastic scatterings from different atomic sites. To properly describe the EDDF, full multiple scattering renormalization is inevitable even at 1000 eV, which needs large scale computations. Temperature effects on the EDDF are also discussed, which smear the EDDF because the quantum interference effects are destroyed because of the thermal motions. We can estimate the mean free path from the asymptotic behavior of $\phi(z)$ for large $z$ where $\ln\phi(z)$ is a linear function of $z$.

## 1. Introduction

X-ray photoelectron spectroscopy (XPS) have developed rapidly, which are now used extensively in many different areas of science and technology [1]. Excited electrons from solids travel some distance before they escape through the solid surface. To describe the attenuation, the inelastic mean free path (IMFP) and the emission depth distribution function (EDDF) are key factors. In several theoretical and experimental studies the EDDF of photoelectrons from s subshells leaving a surface in certain directions exhibits complex behavior, with a maximum at the depth comparable to the IMFP [2-9]. So far, the Monte Carlo simulation has been successfully applied to analyze the EDDF which neglect the quantum interference associated with electron elastic scatterings from composite atoms. It is thus important for us to apply purely quantum approaches to the EDDF calculations in order to study the applicability of the widely used classical methods. Of course quantum calculations must be much harder than the classical ones.

In this paper, we calculate the EDDF based on the many-body quantum mechanical multiple scattering theory developed by us to study photoelectron diffraction spectra [10-13], where the optical potential are explicitly calculated. The present theoretical framework explicitly includes elastic scatterings from each atomic site and damping effects during photoelectron propagation. In the previous paper our discussion is focused on photoemission from Fe crystal [14]. Here we present the results for those from Al crystal.

## 2. Theory

First principle many-body photoemission theories give us a useful formula for X-ray photoelectron diffraction (XPD) amplitude $M(\boldsymbol{k})$ measuring photoelectron momentum $\boldsymbol{k}$ excited from the site $\boldsymbol{R}_A$, which is written by [10,12]

$$M(\boldsymbol{k}) = \sum_{\alpha} e^{-\kappa D_\alpha(\hat{\boldsymbol{k}})} e^{-i\boldsymbol{k}\cdot\boldsymbol{R}_{\alpha A}} \sum_{LL'} Y_{L'}(\hat{\boldsymbol{k}}) \times \left[\left(1 - X(T)\right)^{-1}\right]^{\alpha A}_{L'L} M_{LL_c}, \tag{1}$$

$$X^{\alpha\beta}(T) = t_l^{\alpha}(k) G_{LL'}(k\boldsymbol{R}_{\alpha\beta})(1-\delta^{\alpha\beta}) \times \exp(-k^2\sigma^2_{\alpha\beta}(T)) \tag{2}$$

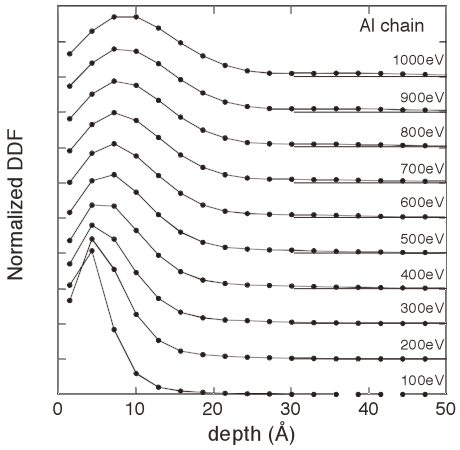


Figure 1: Al 2s EDDF for different $\varepsilon_k$ from 100 to 1000 eV.

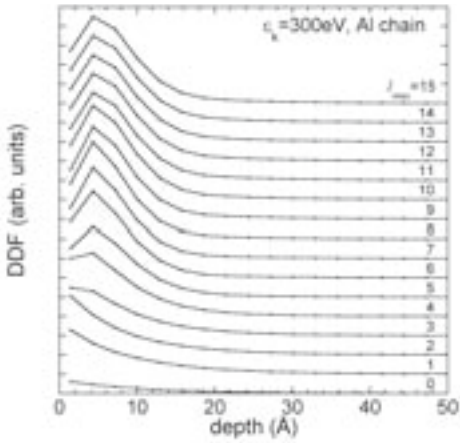


Figure 2: EDDF for different $l_{\max}$ with $\varepsilon_k$ = 300 eV.

where $X$ is a matrix labeled by a set of atomic sites (A, $\alpha, \beta, \cdots$) and orbital angular momentum $L = (l, m)$. The infinite sum over $l$ and $l'$ should be truncated at a finite $l_{\max}$ for practical calculations. The full multiple scattering is taken into account by use of the inverse matrix $(1 - X)^{-1}$. $\sigma^2_{\alpha\beta}(T)$ is Debye-Waller factor at temperature $T$ and $\boldsymbol{R}_{\alpha A} = \boldsymbol{R}_\alpha - \boldsymbol{R}_A$. The explicit formula of the the site-$t$ matrix $t^\alpha_l(k)$, the propagator $G_{L'L}(k\boldsymbol{R}_{\alpha A})$ and the the photoexcitation matrix element $M_{LL_c}$ excited by linearly polarized light parallel to z-axis are found in Ref. [12, 14]. Equation (1) is the basic formula to calculate the photoemission, where we can systematically include the electron attenuation in solid and the thermal vibration [14].

### 3. Calculated Results

In this section we explicitly show some calculated EDDFs for Al surfaces by use of the full multiple scattering approaches described in the previous section.

#### 3-1. One-dimensional Al chain

We first study the EDDF in normal photoemission from the one-dimensional Al chains along the z-axis. We consider the excitation from the Al 2s level irradiated by linearly polarized X-rays parallel to the z-axis. The chain length is 142 Å composed of 50 Al atoms whose interatomic distance is 2.86 Å referring to that in Al fcc crystals. We neglect the Debye-Waller factors here.

Figure 1 shows the EDDF from Al 2s photoemission for different photoelectron energies from $\varepsilon_k$ = 100 to 1000 eV for the chain model. We normalize the EDDF $\phi(z)$ so as to be $\int_0^\infty \phi(z)dz = 1$ where $z$ is the depth of the emitter from the surface. Filled circles show the Al lattice sites from which photoelectrons are ejected. The breakdown of the exponential decay should be caused by the focusing effects as widely observed in XPD [13, 15] and in EXAFS spectra [16]. We clearly find the peak shift to deep side and the peak broadening with the increase of $\varepsilon_k$. For high energy photoemission the contribution from deep sites is important because of large IMFP.

We next investigate $l_{\max}$ dependence of the calculated EDDF, where $l_{\max}$ is the maximum $l$ to be taken into account in the sum over $l$ in eq. (1). Figure 2 shows the $l_{\max}$ dependence for Al 2s photoemission intensity with $\varepsilon_k$ = 300 eV. For $l_{\max}$ = 0 to 3, no peak is observed in the EDDF, whereas a peak is observed when $l_{\max} \geq 5$. We find a good convergence for $l_{\max}$ = 10; larger $l_{\max}$ gives no prominent difference in the EDDF. In comparison with the result for Fe surfaces, we should use nearly the same $l_{\max}$ even though Fe is much heavier than Al. This result is also related to the focusing effects: We expect the strong focusing effects for large $l_{\max}$, which can give the larger photoemission intensity from the second layer than that from the first layer. Small $l_{\max}$ cannot describe the focusing effects. For the photoemission from the deeper sites the exponential damping plays more important role than the forward elastic scatterings.

#### 3-2. Three-dimensional model

In this subsection we use more realistic models than the chain models considered before where we only consider the forward and the backward scatterings in the chain. In addition to them we also consider elastic scatterings with small angles; surrounding atoms around the

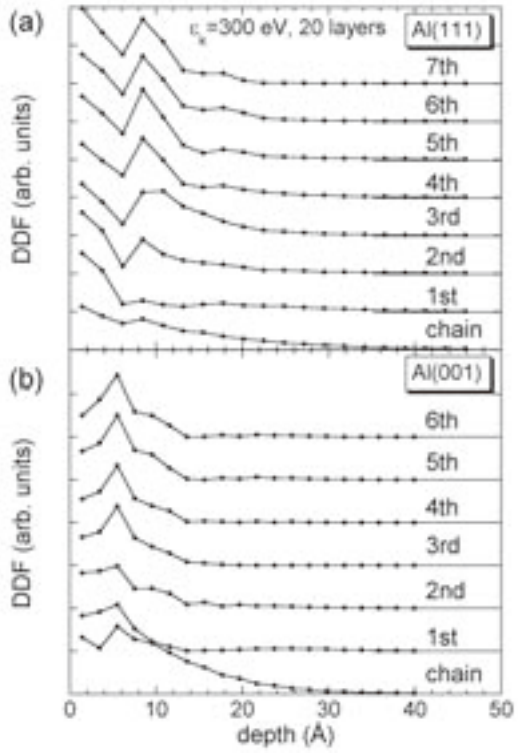


Figure 3: Calculated EDDFs from Al (111) surface (a) and (001) surface (b) where we use cylindrical models with different radii for $\varepsilon_k$ = 300 eV. The horizontal lines on the right side describe the baselines of the EDDF $\phi(z)$ for each size.

z-axis in a finite size cylinder are taken into account. All multiple scatterings inside these cylindrical clusters are fully taken into account. We consider the photoemission from Al (111) and (001) surfaces neglecting the Debye-Waller factors. We change the cylinder radius up to the 7th sheet around the emitter atoms for (111) surface and 6th sheet for (001) surface. The calculated results for these models are shown in Fig. 3; the EDDF depends on the detail of the surface structure. A peak is observed at the 4th layer in case of (111) surface which consists of A-B-C-A-B-C- periodic array and the emitter on the 4th layer has a scatterer just above it which gives rise to the forward focusing enhancement.

On the other hand the calculated EDDF from (001) surface has a peak at 3rd layer because it consists of A-B-A-B- periodic array. We found the similar result in the photoemission from bcc iron (001) models [14]. In both cases the EDDF shows more rapid decay in cylinder models than in chain models.

### 3-3. Temperature dependence

We next study the temperature dependence of the

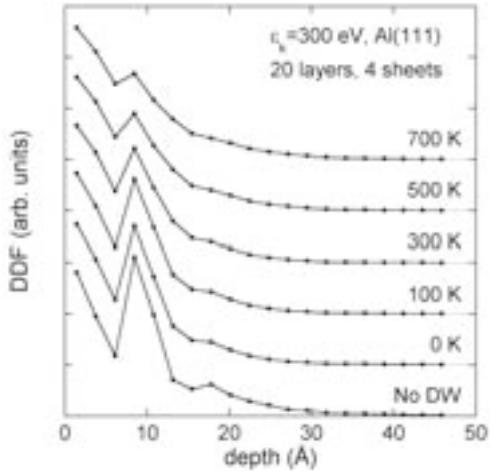


Figure 4: Temperature dependent EDDF from the fcc cylinder model $Al_{205}$ with $\varepsilon_k$ = 300 eV. For comparison the result with no Debye-Waller factor is also shown (No DW)

EDDF for the cylinder models. For the present studies we calculate the Debye-Waller factors in the Debye approximation, where we use $\Theta_D$ = 428 K for Al crystals. Figure 4 shows the temperature dependence of the EDDF for the Al cylinder models including 205 atoms in the cylinder (20 layers and 4 sheets). The temperature varies from 0 to 700 K. Even at 0 K zero-point oscillation makes difference from the result where the Debye-Waller factor is completely neglected. For lower temperature the peak is sharp, which reflects the importance of elastic scatterings to give the prominent peak: The Debye-Waller factor destroys the interference.

### 3-4. EDDF at large $z$

The asymptotic behavior of $\phi(z)$ at large $z$ is well described by a simple exponential law $\phi(z) \sim \phi_0 \exp(-z/\lambda_d)$, where $\lambda_d$ is a dressed IMFP which effectively includes the elastic scattering effects, because the EDDF $\phi(z)$ already include both damping and elastic scattering effects. Of course this law does not work at small $z$ as seen in the previous subsections. Figure 5 shows the calculated $\phi(z)$ as function of the depth $z$ for $\varepsilon_k$ = 100 eV and 300 eV. We use the cylinder model where only the nearby sheet is taken into account (80 layers) because of the computation cost. This figure clearly shows that the approximated exponential formula works well for large $z$ but $\lambda_d$ is not simply $\lambda$, because elastic scatterings are renormalized in the exponential decay formula. The linear fitting provides $\lambda_d$ for different energies, which are listed in Table 1. The $\lambda_d$ is fitted in the depth range of 120 - 160 Å. Ta-

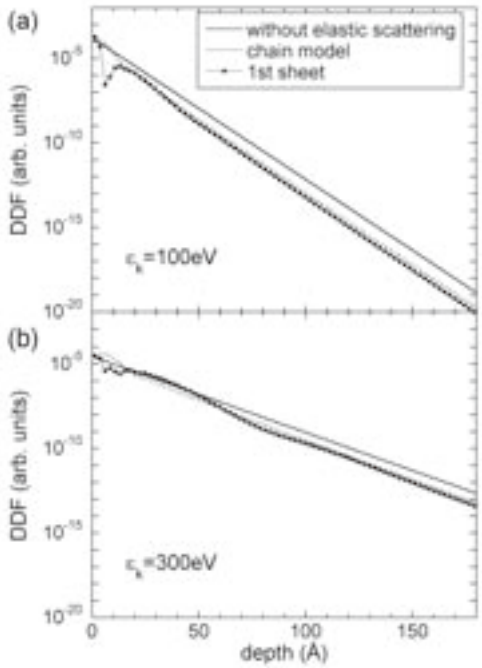


Figure 4: EDDF $\phi(z)$ for photoelectron energies $\varepsilon_k$ = 100 (a) and 300 eV (b) for the chain model and the cylinder model with the first nearby sheet. Simple exponential EDDF $\exp(-z/\lambda)$ without scatterings from surrounding atoms are also shown by solid lines just for comparison.

numa *et al*. have used Penn's algorithm to calculate IMFP in a wide range of materials. The latest version of the IMFP formula proposed by Tanuma *et al.* (TPP-2M) is one of the most frequently used predictive formula to calculate IMFP [17]. In Table 1 the IMFP $\lambda_{\mathrm{TPP}}$, calculated by the TPP-2M formula [17], is also shown for comparison. We find that $\lambda > \lambda_d$ for all energies considered here. Similar behaviors have also been observed in the Monte Carlo simulation [4, 5, 8].

## 4. Concluding Remarks

In this work, we study the EDDF of Al by use of quantum mechanical full multiple scattering calculations. Our calculations give a prominent peak in the EDDF caused by the focusing effects in the forward elastic scatterings, as observed in XPS and EXAFS. The interference can be destroyed by thermal motion of composite atoms, which gives the duller peak with increase of temperature. We obtained the important characteristics of the decaying behavior of $\phi(z)$ at large $z$: Dressed IMFP $\lambda_d$ is smaller than the IMFP $\lambda$ without scattering effects. The other important fact is that the EDDF depends on the surface structure, which is not considered in the jellium model calculations.

Table 1: The bare IMFP $\lambda$, Tanuma's IMFP $\lambda_{\mathrm{TPP}}$ and the dressed ones $\lambda_d$ for Al (111) surface at different $\varepsilon_k$ from 100 to 1000 eV.

| $\varepsilon_k$ (eV) | $\lambda$ (Å) | $\lambda_{\mathrm{TPP}}$ (Å) | $\lambda_d$ (Å) | |
|---|---|---|---|---|
| | | | chain | cylinder |
| 100 | 5.18 | 4.20 | 5.11 | 5.07 |
| 200 | 7.40 | 6.22 | 7.25 | 7.20 |
| 300 | 9.65 | 8.11 | 9.40 | 8.95 |
| 400 | 11.84 | 9.91 | 11.47 | |
| 500 | 13.96 | 11.64 | 13.45 | |
| 600 | 16.03 | 13.31 | 15.36 | |
| 700 | 18.06 | 14.94 | 17.22 | |
| 800 | 20.04 | 16.53 | 19.02 | |
| 900 | 21.99 | 18.09 | 20.78 | |
| 1000 | 23.92 | 19.63 | 22.51 | |

## References

[1] S.Hüfner, *Photoelectron Spectroscopy, Principles and Applications*, 3rd Edn., Springer, New York (2003)
[2] A. Jablonski and H. Ebel, *J. Chem. Phys.* **11**, 627 (1988)
[3] A. Jablonski and J. Zemek, *Surf. Sci.* **347**, 207 (1996)
[4] I. S. Tilinin, A. Jablonski, J. Zemek, and S. Hucek, *J. Elect. Spect. Relat. Phenom.* **87**, 127 (1997)
[5] S. Hucek, J. Zemek, and A. Jablonski, *J. Elect. Spect. Relat. Phenom.* **85**, 257 (1997)
[6] A. Dubus, A. Jablonski, and S. Tougaard, *Prog. Surf. Sci.* **63**, 135 (2000)
[7] J. Zemek, P. Jiricek, S. Hucek, A. Jablonski, and B. Lesiak, *Surf. Sci.* **473**, 8 (2001)
[8] J. Zemek, P. Jiricek, and K. Olejnik, *Surf. Sci.* **572**, 93 (2004)
[9] A. Jablonski, *Surf. Sci.* **586**, 115 (2005)
[10] T. Fujikawa, *J. Phys. Soc. Jpn.* **50**, 1321 (1981)
[11] T. Fujikawa, *J. Phys. Soc. Jpn.* **51**, 251 (1982)
[12] T. Fujikawa, *J. Phys. Soc. Jpn.* **54**, 2747 (1985)
[13] C. S. Fadley, *Synchrotron Radiation Research, Advances in Surface and Interface Science*, Vol. 1, ed. by R. Z. Bachrach, Plenum, New York (1992)
[14] H. Shinotsuka, H. Arai, and T. Fujikawa, *Phys. Rev. B* **77**, 085404 (2008)
[15] W. F. Egelhoff, *J. Vac. Sci. Technol. A* **6**, 730 (1988)
[16] J. J. Rehr and R. C. Albers, *Rev. Mod. Phys.* **72**, 621 (2000)
[17] S. Tanuma, C. J. Powell, and D. R. Penn, *Surface Interface Anal.* **17**, 911 (1991).